 doi:10.20944/preprints201905.0287.v1

Peer-reviewed version available at *Remote Sensing* **2019**, *11*, ; doi:10.3390/rs11131580

Accounting for wood, foliage properties and laser effective footprint in estimations of Leaf Area Density from multiview-LiDAR data

François Pimont
UR629 INRA, Avignon, France, francois.pimont@inra.fr
Maxime Soma
UR629 INRA, Avignon, France, maxime.soma@inra.fr
Jean-Luc Dupuy
UR629 INRA, Avignon, France, jean-luc.dupuy@inra.fr

Abstract

The amount and spatial distribution of foliage in a tree canopy have fundamental functions in ecosystems as they affect energy and mass fluxes through photosynthesis and transpiration. They are usually described by the Leaf Area Index (LAI) and the Leaf Area Density (LAD), which can be measured through a variety of methods, including voxel-based methods applied to LiDAR point clouds.

A theoretical study recently compared the numerical errors arising from different voxel-based estimation methods for Plant Area Density (PAD) based on Beer's law-based, contact frequency and Maximum-Likelihood Estimation, showing that the bias-corrected Maximum Likelihood Estimator was theoretically the most efficient. However, this earlier study i) ignored wood volumes; ii) neglected vegetation clumping inside the voxel; iii) ignored instrument characteristics in terms of effective footprint, iv) was limited to a single viewpoint. In practice, retrieving LAD from PAD is not straightforward, vegetation is not randomly distributed in volumes of interest, beams are divergent and forestry plots are usually sampled from more than one viewpoint, to mitigate the effect of occlusion.

In the present short communication, we extend the previous efficient formulation to actual field conditions to i) account for the presence of both wood volumes and wood hits, ii) rigorously

Preprints (www.preprints.org) | NOT PEER-REVIEWED | Posted: 24 May 2019 doi:10.20944/preprints201905.0287.v1

Peer-reviewed version available at *Remote Sensing* **2019**, *11*, ; doi:10.3390/rs11131580

include correction terms for vegetation and instrument characteristics, iii) integrate multiview data. A numerical comparison with other methods commonly used to combine information from different viewpoints led to error reduction, especially in poorly-explored volumes, which are frequent in actual canopies. Beyond its concision, completeness and efficiency, this new formulation -which can be applied to multiview TLS, but also UAV LiDAR scanning- can help reducing errors in LAD estimation.

Keyword: bias, efficiency, element size, LAD, LAI, leaf and wood separation, LiDAR, multiple viewpoints, point cloud, TLS, UAV, voxel

1. Introduction

The amount and spatial distribution of foliage in a tree canopy have fundamental functions in ecosystems as they affect energy and mass fluxes through photosynthesis and transpiration (Norman and Campbell, 1989). Terrestrial LiDAR (Light Detection And Ranging), hereinafter referred to as TLS (Terrestrial Laser Scanning) recently emerged as a promising tool to estimate leaf/plant area density (LAD/PAD) distribution for individual plants and forest plots (Yan et al. 2019, for a review). The approach is most often based on a traversal algorithm, which enables to compute the hits and "free paths" (i.e. distance travelled without interception) sampled by each beam in a given volume, which can be either voxels or crown volumes, and to derive different metrics to estimate the quantity of interest (e.g. Béland et al. 2011; Pimont et al. 2015; Bailey and Mahafee 2017a; Hu et al. 2018; Soma et al. 2018).

Among the different metrics suggested in the past, a recent comprehensive theoretical study (Pimont et al. 2018) has shown that the Modified Contact Frequency, first introduced in Béland et al. (2011), corresponds to the Maximum Likelihood Estimator "MLE" (Kay 1993) of the attenuation coefficient. This attenuation coefficient is the rate at which the point cloud density decays with vegetation interception, which is related to the LAD/PAD linearly, contrary

Peer-reviewed version available at Remote Sensing 2019, 11, ; doi:10.3390/rs11131580

to the transmittance or the gap fraction used in Beer's law-based methods. To date Beer's law-based methods, which inverts the transmittance equation, are still more popular than the MLE (Yan et al. 2019), while they do not take full advantage of the tridimensional information available in the point cloud, by ignoring free paths, and leads to additional complexity in the inversion when path length is not constant (Béland et al. 2014b; Pimont et al. 2018). This trend can probably be explained by the strong legacy of gap fraction approaches in this research field. The benefits of the MLE are that the formulation is more straightforward and efficient, without making assumption on the geometry of the volume of interest (Pimont et al. 2018). The method simply provides the most likely estimate of the attenuation coefficient, given the observation of free paths and hits, simply assuming that explored and unexplored regions exhibit similar random distributions of vegetation elements. The MLE approach, which relies on free paths, should not be confused with the PATH method (Hu et al. 2014; Hu et al. 2018), which uses the path-length distribution to identify crown volumes, in order to mitigate the impact of clumping in crown volumes, and which has to date only been applied to Beer's law-based methods. One could notice, that the PATH method could be combined with MLE instead.

One limitation of the MLE as is, -but also of Beer's law based methods-, is their biasness when the number of beams exploring a given voxel is limited (typically smaller than 30), or when vegetation elements are not small with respect to voxel size. Such biases can be theoretically corrected, leading to a bias-corrected MLE which is "efficient", in the sense that it is unbiased and it exhibits the smallest variability theoretically reached by any unbiased estimator (Pimont et al. 2018).

This estimator, however, is based on theoretical assumptions: vegetation elements are assumed to be randomly distributed within volumes and TLS beams are infinitely thin. Hence, it typically requires additional corrections when applied to actual point clouds to account for LiDAR effective footprint in clumped vegetation elements (e.g. Soma et al. 2018), similarly to

Preprints (www.preprints.org) | NOT PEER-REVIEWED | Posted: 24 May 2019 doi:10.20944/preprints201905.0287.v1

Peer-reviewed version available at Remote Sensing 2019, 11, ; doi:10.3390/rs11131580

other methods applied to voxels or tree crowns (Béland et al. 2011; Béland et al. 2014a; Hu et al. 2018; Yan et al. 2019). Also, the theoretical formulation presented in Pimont et al. (2018) neglects the presence of woody elements in the estimation of LAD, which should be accounted for separately, either using a separation between leaf and wood returns (Béland et al. 2011; Béland et al. 2014a) or "leaf-off" scans (Soma et al. 2018; Hu et al. 2018). To date, a theoretical framework for such inclusion is still missing. Another limitation of the theoretical formulation is that it was applied to an individual scan, whereas field applications often require the use of multiple viewpoints to mitigate the impact of vegetation occlusion. Several methods have been suggested to combine the information arising from the different scans, such as relying on the best viewpoint on a given voxel (i.e. the one with maximal beam number, Côté et al. 2011), combining all hits as if they belonged to the same scan (Béland et al. 2011), or weighting estimates from each scan according to the number of beams of each viewpoint (Pimont et al. 2015; Hu et al. 2018). To date, the consequences of such combinations on LAD estimation have never been studied.

In the present short communication, we present a bias-corrected Maximum Likelihood Estimator for the LAD with multiview-LiDAR data in volumes of interest, which naturally extends the formulation presented in Pimont et al. (2018) to actual field data, with the presence of wood volumes, wood hits, correction terms to account for beam divergence and vegetation clumping, as well as to multiview data. The method is applied to an example virtual vegetation scene, and is compared to other common techniques used to combine information from different viewpoints, presented in Appendix C for brevity.

2. Background and limitations of existing methods

The theoretically-bias corrected estimator (TBC-MLE, from Pimont et al. 2018 and Soma et al. 2018)

Here, we briefly summarize the *PAD* estimation in the mathematical framework proposed by Pimont et al. (2018), in which a correction factor was included to account for the effective footprint in clumped vegetation (Soma et al. 2018). This factor H varies with the distance of measurement and the voxel size. Observations suggest that H decreases with distance to scanner, to compensate the increase in effective footprint caused by beam divergence and variation in return detection, which induces an increase of the apparent area of vegetation elements (Béland et al. 2014a; Soma et al. 2018). Also, H increases with the voxel size, to compensate the effect of vegetation clumping inside voxels, which causes discrepancies to the theoretically random distribution of vegetation elements, as a consequence of Jensen's convexity inequality (Béland et al. 2014a; Bailey and Mahafee 2017a; Soma et al. 2018). It also depends on the scanner and to a lesser extent, on vegetation caracteristics (Soma et al. 2018), although the element size and shape can at least partially be accounted for, through the notion of "effective" free path z_e (Pimont et al. 2018, see Eq. 3 below and Appendix A).

When H is known (for example from laboratory experiments in Soma et al. 2018) and the projection function G is separately estimated (e.g. Béland et al. 2011; Bailey and Mahafee 2017b), the *PAD* in a single voxel from a single viewpoint can be estimated as follows:

$$\widetilde{PAD} = \frac{H}{G}\tilde{\Lambda} \tag{1}$$

where $\tilde{\Lambda}$ is an estimator of the attenuation coefficient, G is the leaf projection factor, and H is the correction factor for both voxel size and distance to scanner.

For a given viewpoint, the attenuation coefficient can be estimated from the Maximum Likelihood estimator (MLE). It is equal to the number of hits Ni divided by the sum of free paths Σz (**Fig. 1**), which are computed with a traversal algorithm.

$$\tilde{\lambda} = \frac{Ni}{\Sigma z} \tag{3}$$

The free path sum is the total distance actually travelled by beams inside a voxel, before their eventual interceptions by a vegetation element, which can be either leaf or wood (**Fig. 1**).

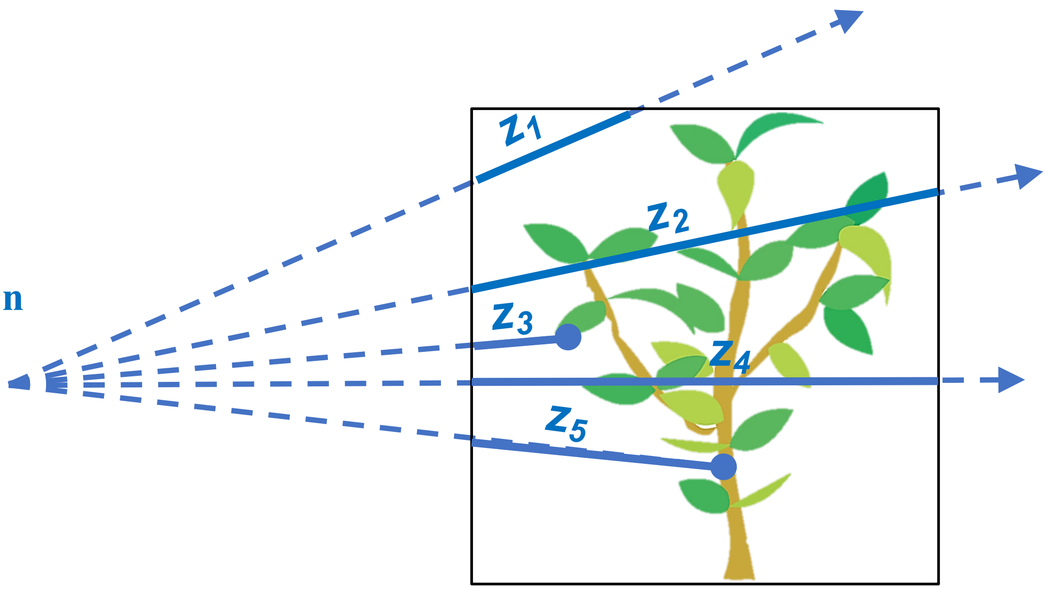

Figure 1. Scheme of the information provided by the traversal algorithm which is used to compute the MLE of the attenuation coefficient: number of hits *Ni* (blue dots) and free paths (distances *z* travelled by the beams, blue lines) in each voxel. The dotted lines represent pulse trajectory.

This first estimator is similar to the Modified Contact Frequency introduced in Béland et al. (2011). Such estimator is biased when the beam number is low or when vegetation elements are not infinitely small and can be corrected with a more sophisticated estimator $\tilde{\Lambda}$, referred to as the theoretically-bias corrected MLE (TBC-MLE, Pimont et al. 2018, Soma et al. 2018). In this estimator, each free path z is replaced by the effective free path z_e:

$$z_e = -\frac{log(1-\lambda_1 z)}{\lambda_1} \qquad (3)$$

where λ_1 is the attenuation coefficient of a single element of vegetation (see appendix A for an estimation of λ_1 for cylindrical needles or elliptical flat leaves). Obviously, $z_e \approx z$ when λ_1 is very small (i.e. the turbid medium assumption).

Preprints (www.preprints.org) | NOT PEER-REVIEWED | Posted: 24 May 2019 doi:10.20944/preprints201905.0287.v1

Peer-reviewed version available at Remote Sensing 2019, 11, ; doi:10.3390/rs11131580

For the purpose of the present study, the TBC-MLE of the PAD (Soma et al. 2018) is slightly rearranged, to ease generalization to multiple viewpoints, which is proposed in the next section:

$$\widetilde{PAD} = \frac{H}{G}\tilde{\Lambda} = \frac{H}{G\sum z_e}\left(\mathrm{Ni} - \frac{\sum_{hits} z_e}{\sum z_e}\right) \tag{4}$$

In Eq. 4, Ni is the number of hits in the voxel, whereas Σz_e is the effective free path sum, and $\Sigma_{hits} z_e$ is the effective free path sum for beams with hits inside the voxel (hence $\frac{\Sigma_{hits} z_e}{\Sigma z_e}$ ranges between 0 and 1). The second term in brackets corresponds to the bias-correction term suggested in Pimont et al. (2018), which can be neglected when the beam number is high (i.e. larger than 30). This estimator is unbiased when N>5 and reaches the Cramer-Rao bound, meaning it is the most efficient unbiased estimator, given the available information (Pimont et al. 2018).

In this formulation, HNi is close to the number of hits centered on a leaf, first introduced in Béland et al. (2011) to account for beam divergence. The overall formulation, however, is slightly different, since Béland et al. (2011) ignored beams with partial hits in the free path sum. In section 3, we rigorously incorporate H and G in the mathematical derivations.

Theoretical variance and 68% confidence interval of the TBC-MLE

Mathematical derivations presented in Pimont et al. (2018) led to an estimator of the variance of $\widetilde{PAD}$. Such variance estimator is useful to quantify the accuracy of a given LAD estimate, in terms of random errors caused by LiDAR sampling in the voxel (which magnitude decreases with beam number N):

$$\sigma^2_{\widetilde{PAD}} = \left(\frac{H}{G}\right)^2 \sigma^2_{\tilde{\Lambda}} = \frac{1}{Ni}\left(\frac{1}{G/H\Sigma z_e}\left(Ni - \frac{\sum_{hits} z_e}{\sum z_e}\right)\right)^2 \tag{5}$$

Peer-reviewed version available at Remote Sensing 2019, 11, ; doi:10.3390/rs11131580

In Eq. 5, the contribution of the variance due to the variability of element positions in a vegetation sample is neglected for simplicity. For the interested reader, an empirical model for this quantity was presented in Pimont et al. (2018), in the case of "square flat" leaves.

A related metric of interest is the radius of the 68% confidence interval of the LAD estimate, which is given by (Pimont et al. 2018):

$$\Delta\widehat{PAD} = \frac{H}{G}\Delta\tilde{\Lambda} = \frac{1}{G/H}\frac{Ni + \frac{1}{2} - \frac{\sum_{hits} z_e}{\Sigma z_e}}{\sqrt{Ni + \frac{1}{2}\Sigma z_e\left(1 + \frac{1}{N}\right)}} \quad (6)$$

The rationale for the ½ terms is to avoid that the confidence interval radius equals 0 when Ni = 0, which would be incorrect (indeed, there is non-zero chance that additional beams hit some potential vegetation elements). This confidence interval is referred to as "Agresti-Coull" in Pimont et al. (2018) and leads to a lower bound of $\frac{1}{\sqrt{2}\Sigma z_e\left(1+\frac{1}{N}\right)}$ when Ni=0. It expresses that the estimation is more accurate as Σz_e increases, but never reaches 0, even for a high number of beams *N*.

Accounting for wood returns

As most applications focus on LAD -not PAD-, several methods have been developed to account for wood elements. For example, the authors of Béland et al. (2011) counted only hits related to leaf, thanks to a separation of leaf and wood returns based on return intensity. This is equivalent to the introduction of a multiplicative factor equals to the leaf hit fraction *F*:

$$F = \frac{\mathrm{Ni}^l}{\mathrm{Ni}} \quad (7)$$

However, as for the beams for which hits were not centered on the leaf, free paths corresponding to wood returns were ignored in the sum of free path in Béland et al. (2011).

Another approach was to determine the *LAD* as a difference between "leaf on" and "leaf off" conditions (Soma et al. 2018; Hu et al. 2018). This approach relies on the implicit assumption

Peer-reviewed version available at Remote Sensing 2019, 11, ; doi:10.3390/rs11131580

that the total attenuation coefficient of vegetation elements is the sum of the attenuation coefficients of respectively leaf and wood elements, which requires an assumption of random distribution for both leaf and wood elements, which is obviously incorrect in the case of logs or large branches.

In both approaches, the volume occupied by logs and branches inside voxel was neglected. In section 3, we rigorously include wood volumes and leaf hits in the mathematical derivations.

Multiview estimation

When several points clouds are available (each with an index $j \in [1;J]$), the most basic method to deal with multiview data is to select the "best viewpoint" (i.e. the scan j, which sampled a given voxel with the highest number of beams N_j), as in Côté et al. (2011). This estimator, here shown for an *LAD* estimator, referred to as "*Nmax*", is defined as:

$$\widetilde{LAD}^{Nmax} = \widetilde{LAD}_{jmax}, \text{ with } jmax \text{ so that } N_{jmax} = \max_{j \le J} N_j \quad (8)$$

This approach is unbiased, provided that each individual estimator is unbiased (e.g. when $N > 5$ with the TBC-MLE, Pimont *et al.* 2018). However, information from other scans is ignored, which is not optimal, especially when several viewpoints explore a given voxel with similar numbers of beams.

A more sophisticated method, referred to as "*N-weighted*" (NW) is based on a weighted average of each estimates $\widetilde{LAD}_j$ (from the different viewpoints), the weights being equal to N_j, as suggested in Hu et al. (2018):

$$\widetilde{LAD}^{NW} = \frac{1}{\sum_{j \le J} N_j} \sum_{j \le J} N_j \, \widetilde{LAD}_j \quad (9)$$

No information is ignored with this second approach, since all viewpoints contribute to the final estimation.

Peer-reviewed version available at Remote Sensing 2019, 11, ; doi:10.3390/rs11131580

In section 3, we rigorously collect the information from different view points in the mathematical derivations.

3. Generalized Maximum-Likelihood Estimation for LAD from multiview-LiDAR data

The generalized formulation

This section details our new formulation of the estimation of Leaf Area Density from multiview-LiDAR data within a volume of interest, which can be either a voxel or a crown volume, but it is simply referred to as "the voxel" for simplicity. It relies on similar assumptions as above, with three noticeable differences. First, we explicitly consider the subvolume V_w of the voxel V occupied by wood elements (**Fig. 2**). Within a voxel volume V, we assume that small leaf elements are randomly distributed in the subvolume $V - V_w$ of V, which is not occupied by the wood. This subvolume containing the leaf elements has a volume fraction equals to:

$$\alpha = 1 - \frac{V_w}{V} \tag{10}$$

In general, α is very close to 1, except when large branches or logs intersect the voxel. Here, no specific assumption is made on the topology of the wood volume V_w , neither on how it is distributed with respect to the volume $V - V_w$ in which leaves were present.

Peer-reviewed version available at *Remote Sensing* **2019**, *11*, ; doi:10.3390/rs11131580

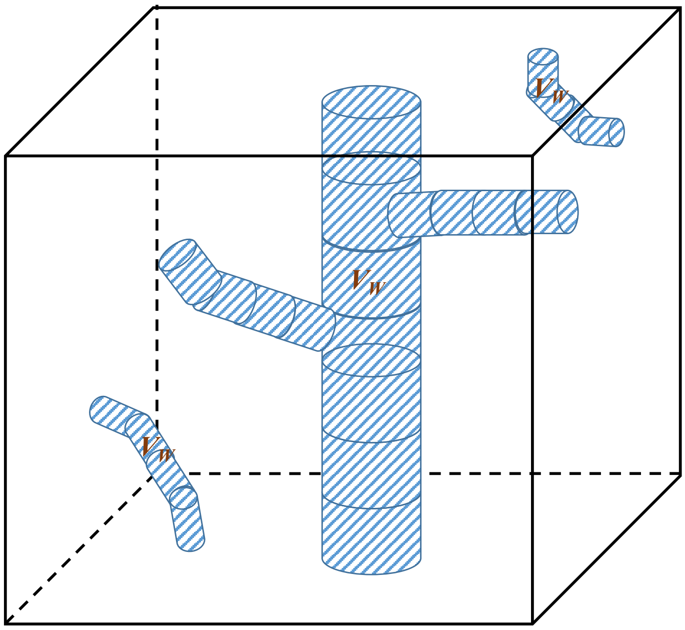

Figure 2. Scheme of the representation of wood volumes V_w (in dashed blue), in the voxel of volume V. We assume that leaf elements are randomly distributed in volume $V - V_w$, which exhibits a very complex and unknown topology.

Second, we assume that the effective attenuation coefficient in $V - V_w$, which corresponds to what is actually viewed by the scanner from viewpoint j, verifies $\lambda_j = \frac{G_j LAD}{H_j}$ and that the factors for effective footprint on clumped vegetation H_j and for leaf projection G_j are known. Third, we assume that J point clouds are available (each with an index $j \in [1; J]$). It is important to acknowledge that correction factors can exhibit large variations with scanner position j given voxel, as distances to scanner and/or view angle differ.

In appendix B, we apply similar mathematics as in Pimont et al. (2018) to leaf elements distributed inside $V - V_w$. For consistency with usual definitions, the *LAD* is still defined as the surface area of leaf elements divided by the voxel volume V, despite the leaves are not distributed in the whole volume V. This explains the presence of volume fraction α in the following equations. From the distribution of "multiview" leaf hits, free paths, projection and correction factors, the objective here is to determine the most likely value of *LAD* (MLE), given

Preprints (www.preprints.org) | NOT PEER-REVIEWED | Posted: 24 May 2019 doi:10.20944/preprints201905.0287.v1

Peer-reviewed version available at Remote Sensing 2019, 11, ; doi:10.3390/rs11131580

the observations. The mathematical derivations slightly differ from Pimont et al. (2018), since there is not a single attenuation coefficient λ for which the MLE can be computed, but as many attenuation coefficients λ_j as viewpoints j. We thus directly compute the Maximum Likelihood Estimator "MLE" of the *LAD* (i.e. not of the attenuation coefficient λ), which cancels the first derivative of log-likelihood (Kay, 1993, chapter 7) of the LAD and find (Eq. B6):

$$MLE_{LAD}^{M} = \alpha \frac{\mathrm{Ni}^{l}}{\sum \frac{G}{H} z_e} \tag{11}$$

where $Ni^l = \sum_j Ni_j^l$ is the total number of leaf hits (for all scans) and $\sum \frac{G}{H} z_e = \sum_{j=1}^{J} \sum_{i=1}^{N_j} \frac{G_j}{H_j} z_{e\,j}^{\,i}$ is the sum of the products $\frac{G_j}{H_j} z_j^i$ for beams exploring $V - V_w$ (**Fig. 3**). The "M" superscript corresponds to "Multiview". Here, it is important to notice that, according to the mathematics, wood hits are ignored in the count of hits, but not in the free-path sum, contrary to what was suggested in Béland et al. (2011). Also, the correction factor $\frac{G}{H}$, which accounts for differences between viewpoints, appears as a multiplicative factor in the free path sum. Hence, all hits should be considered equally in the hit sum, no matter the distance to scanner or the view angle, but the free paths should be modified to account for these differences. As for the wood hits, this slightly differ from the "center leaf hit" method presented in Béland et al. (2011, 2014).

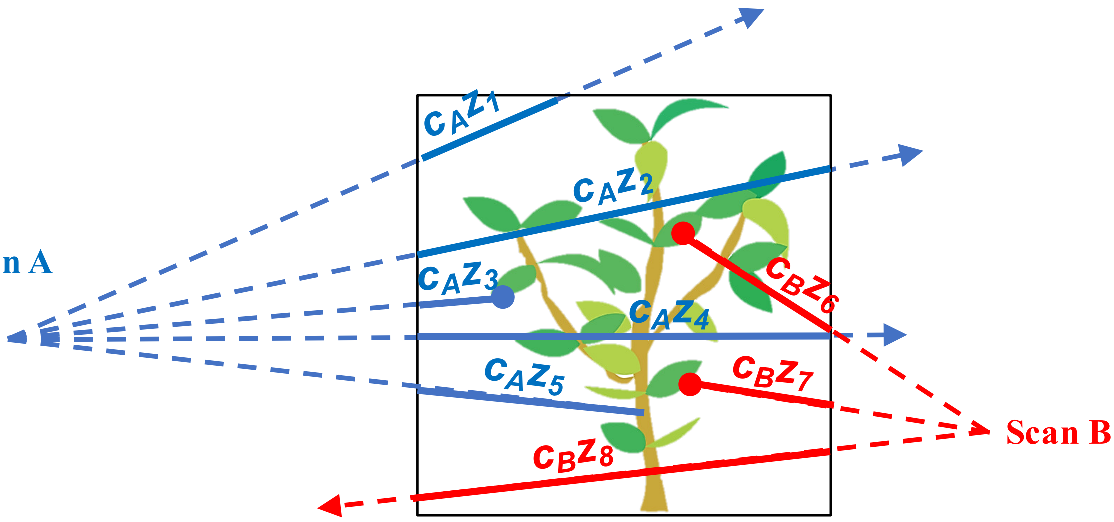

Peer-reviewed version available at Remote Sensing 2019, 11, ; doi:10.3390/rs11131580

Figure 3. Scheme of the information provided by the traversal algorithm which is used to compute the MLE of *LAD* from multiview data from Scan A (in red) and Scan B (in blue): leaf hits (blue and red dots) and free paths (distances z travelled by the beams, blue and red lines) in the voxel. The dotted lines represent pulse trajectories. c_A and c_B represent the correcting factors for viewpoints A and B, which differs with distance to scanner and view angle. For simplicity, correction for effective free path (z_e, Eq. 3) is ignored. NB: in this framework, no leaf can be distributed within the volume V_W occupied by wood elements (in brown). Also, and contrary to Fig. 1, the hits corresponding to woody elements (e.g. 5$^{\text{th}}$ beam of scan 1) are ignored in the hit sum, but the corresponding free paths are accounted for the free-path sum, in which c_A and c_B are used as multiplicative factors.

As for a single viewpoint, this "MLE" is biased when the number of beams is low and a correction can be computed (Pimont et al. 2018). Generalizing this correction to the multiview LAD estimator ("*M*") led to (Appendix B):

$$\widehat{LAD}^M = \frac{\alpha}{\sum \frac{G}{H} z_e}\left(\mathrm{Ni}^l - \frac{\sum_l \frac{G}{H} z_e}{\sum \frac{G}{H} z_e}\right) \tag{12}$$

With $\sum_l \frac{G}{H} z_e$ corresponding to the sum of $\frac{G_j}{H_j} z_j^i$ for beams corresponding to <u>leaf hits only</u>. This formulation obviously generalized the single-scan estimator $\widehat{LAD}_j$, as rewrote in Eq. 4.

In practice, however, the formulation of Eq. 12 requires to discriminate each hit, depending whether it is foliage or wood in order to compute the bias correction term. A slightly more practical formulation can be achieved assuming that $\sum_l \frac{G}{H} z_e \approx F \sum_{hits} \frac{G}{H} z_e$, with the hit leaf fraction $F = \frac{\mathrm{Ni}^l}{\mathrm{Ni}}$:

Preprints (www.preprints.org) | NOT PEER-REVIEWED | Posted: 24 May 2019 doi:10.20944/preprints201905.0287.v1

Peer-reviewed version available at Remote Sensing 2019, 11, ; doi:10.3390/rs11131580

$$\widehat{LAD}^{M} = \frac{\alpha F}{\sum \frac{G}{H} z_e}\left(\mathrm{Ni} - \frac{\sum_{hits} \frac{G}{H} z_e}{\sum \frac{G}{H} z_e}\right) \tag{13}$$

Similarly, generalizing Eq. 5 and 6, the variance of $\widehat{LAD}^{M}$ is:

$$\sigma_M^2 = \frac{\alpha^2}{\mathrm{Ni}^l \left(\sum \frac{G}{H} z_e\right)^2}\left(\mathrm{Ni}^l - \frac{\sum_l \frac{G}{H} z_e}{\sum \frac{G}{H} z_e}\right)^2 \approx \frac{\alpha^2 F}{\mathrm{Ni}\left(\sum \frac{G}{H} z_e\right)^2}\left(\mathrm{Ni} - \frac{\sum_{hits} \frac{G}{H} z_e}{\sum \frac{G}{H} z_e}\right)^2 \tag{14}$$

and the radius of the 68%-level confidence interval of LAD estimate is:

$$\Delta\widehat{LAD}^{M} = \alpha \frac{\mathrm{Ni}^l + \frac{1}{2} - \frac{\sum_l \frac{G}{H} z_e}{\sum \frac{G}{H} z_e}}{\sqrt{\mathrm{Ni}^l + \frac{1}{2}\sum \frac{G}{H} z_e \left(1 + \frac{1}{N}\right)}} \approx \alpha \frac{F\left(\mathrm{Ni} - \frac{\sum_{hits} \frac{G}{H} z_e}{\sum \frac{G}{H} z_e}\right) + \frac{1}{2}}{\sqrt{F\mathrm{Ni} + \frac{1}{2}\sum \frac{G}{H} z_e \left(1 + \frac{1}{N}\right)}} \tag{15}$$

A numerical experiment to compare multiview formulations

The $\widehat{LAD}^{M}$ differs from the *"Nmax"* multiview combination of $\widehat{LAD}_j$ (Eq. 8), but also from the *"N-weighted"*, which can be shown with a numerical expansion of Eq. 9. Beyond the concision and the mathematical support for Eq. 13, it is important to quantify the error reduction resulting from the new formulation in "field like" conditions. We thus conducted a numerical experiment corresponding to plausible field features, aiming at i) providing a brief validation of the "M" – multiview- estimator of LAD presented above (Eq. 13), ii) comparing its performance with the two usual formulations to combine single-view estimates. All the details regarding this numerical experiment are provided in Appendix C for concision. In brief, we generated a "reference" LAD in a 10-m tridimensionnal mesh grid corresponding to plausible features in terms of LAI, clump size and vertical distribution. We simulated five point clouds from different view points. We then estimated the LAD using the three multiview formulations, after applying a traversal algorithm to each point cloud to compute the different statistics. We found that the new multiview estimator ($\widehat{\mathrm{LAD}}^{\mathrm{M}}$) was only marginally biased, even when the total beam

Preprints (www.preprints.org) | NOT PEER-REVIEWED | Posted: 24 May 2019 doi:10.20944/preprints201905.0287.v1

Peer-reviewed version available at *Remote Sensing* **2019**, *11*, ; doi:10.3390/rs11131580

number was small (<2.2% when $\mathrm{N} < 10$), contrary to the other formulations. For example, the "*N-weighted*" estimates (NW) reached a -15 % bias when $\mathrm{N} < 10$. This poor performance was explained by the biases of some of the single-scan estimates, which typically occurred when less than 5 beams of a given viewpoint explored the voxel (and particularly with only 1 or 2 beams). This situation was in practice quite frequent for voxels in which the total beam number was smaller than 10. Overall errors (expressed in RMSE) were also smaller with $\widetilde{\mathrm{LAD}}^{\mathrm{M}}$, than for two other estimates. In particular, the differences between $\widetilde{\mathrm{LAD}}^{\mathrm{M}}$ and $\widetilde{\mathrm{LAD}}^{\mathrm{Nmax}}$, which were observed for all classes of beam numbers, were consistent with the fact that the information from secondary viewpoints was ignored with *"Nmax"*. RMSE for $\widetilde{LAD}^{NW}$ were more than twice as big as for $\widetilde{LAD}^{M}$, when N was lower than 30. Such differences were caused by infrequent, but very large overestimations observed with $\widetilde{LAD}^{NW}$.

4. Discussion

The present work extends the method of the theoretically-bias-corrected Maximum Likelihood Estimator, initially introduced for the attenuation coefficient (Pimont et al. 2018), to the LAD. The new estimator accounts for vegetation element size, wood volume and hits, correction factors for effective footprint, vegetation clumping and orientation, and multiview data. It can be applied to any volume of interest, which can be for example either a voxel (Soma et al. 2018) or a crown volume (e.g. Hu et al. 2018 with a Beer's law based method). As it naturally incorporates variations in view angle and distance to scanner, it should be applicable to UAV LiDAR data, provided that the traversal algorithm accounts for UAV travel path and that corresponding correction factors are known.

The novelty of the approach presented here lies in the fact that the Maximum Likelihood Estimation is applied directly to the *LAD*, rather than to the attenuation coefficient as in the

Peer-reviewed version available at Remote Sensing 2019, 11, ; doi:10.3390/rs11131580

original method and that wood elements are explicitly considered as a volume in which no leaf can be present. This significant advance was permitted by the fact that the MLE does not assume a particular topology for the volume of interest (Pimont et al. 2018), so that it can be applied to a very complex –and unknown- volume (here, the volume of the voxel which is not occupied by woody elements). On the contrary, Beer's law-based methods cannot be easily applied to an unknown geometry and does not take full advantage of all the information available in free paths (Pimont et al. 2018). In the present formulation, no assumption is made on the relative distribution of leaf and wood, the only assumption being that leaves are randomly distributed in the volume of the voxel that is not occupied by wood. The random distribution assumption is not fully realistic, but discrepancies can be corrected through factors to account for leaf orientation, subvolume clumping and LiDAR effective footprint (Soma et al. 2018), which were rigorously included in the new approach in a straightforward manner. Although presenting strong similarities with the modified contact frequency first implemented in Béland et al. (2011), the mathematical derivations suggest that beams corresponding to wood hits and those corresponding to non-central leaf hits should be accounted for in the free path sum, contrary to what was suggested in the earlier study. Another difference is the manner to account for vegetation element size correction suggested in Béland et al. (2014a), which is also different, as already pointed out in Pimont et al. (2018), with the notion of effective free path (Eq. 3). Much more significant differences should be expected, however, from the difference in free path sum computations, than from the difference in element size corrections.

In our formulation, one of the critical aspect is to be able to estimate a fraction of leaf hits F, as well as the leaf volume fraction α (Eq. 13). The development of algorithms and methods for leaf and wood separation is a subject of active research (e.g. Takoudjou et al. 2018; Wang et al. 2018; Xi et al. 2018), which is a prerequisite to most methods aiming at retrieving wood volume (e.g. Raumonen et al. 2013). One could notice that determining the leaf fraction

 doi:10.20944/preprints201905.0287.v1

Peer-reviewed version available at *Remote Sensing* **2019**, *11*, ; doi:10.3390/rs11131580

F is less challenging that the classification of each individual hit as "leaf" and "wood", in the sense that leaf fraction can be correctly estimated from a classification method which can exhibit significant omission/commission errors. In particular, the leaf fraction can be estimated on a subset of the point cloud, which could help to save computational resources. The correction factor α for wood volumes can probably be neglected in most situations corresponding to foliage, since bulk density of thin twigs are on the order of 0.1 kgm^{-3}, which corresponds to volume fraction on the order of 0.02 (Keane et al. 2005). However, such a correction is likely to be necessary when trunks or branches intersect the voxel, otherwise leading to *LAD* overestimation, even if the leaf fraction *F* is correctly estimated. In this context, tree models derived from LiDAR data (e.g. Raumonen et al. 2013) can provide the appropriate information.

Our numerical experiment enabled a theoretical validation of the new estimator in a simplified, but plausible context, as well as a comparison with other simple formulations used to combine multiview data, thanks to well-defined references (Yan et al. 2019). This numerical experiment extended the ones of Pimont et al. (2018), since the ray tracing and the traversal algorithms were applied within a virtual, but more realistic forestry plot, as in Grau et al. (2017) or Soma et al. (2019), rather than within individual voxels. We found that the multiview estimator performed better than the "*Nmax*" and "*N-weighted*" formulations, without requiring any additional complexity. Such a result was expected in terms of errors for the "*Nmax*", since this basic approach ignored the information provided by secondary viewpoints. On the contrary, the counter performance of the "*N-weighted*" was relatively unexpected, leading to much higher errors, because of infrequent, but very large overestimations, when one of the poor viewpoints led to an outlier.

This later point highlights the importance of the use of unbiased estimators. More generally, the unbiasness and efficiency of estimators in the inner-canopy where point density is low is critical (Yan et al. 2019). Indeed, the numerical experiment presented in Appendix C confirms that the distributions of beam numbers in voxels at various heights is very heterogeneous (**Fig. 4**). Above 6 meters, and up to the top of the canopy, the percentages of unexplored or poorly-explored voxels were very high. Of course, such statistics are highly dependent on the number of scans (here 5), the scanner angular resolution (here 0.036°) and the grid size (here 0.1 m). Such sensitivities, as well as their consequences on estimation accuracy are analyzed in details in Soma et al. (2019) and are beyond the scope of the present short communication, which aimed at presenting the new estimator. It was relevant, however, to recall the frequent occurrence of poorly-explored voxels, to highlight the importance of the results of the numerical experiment presented here.

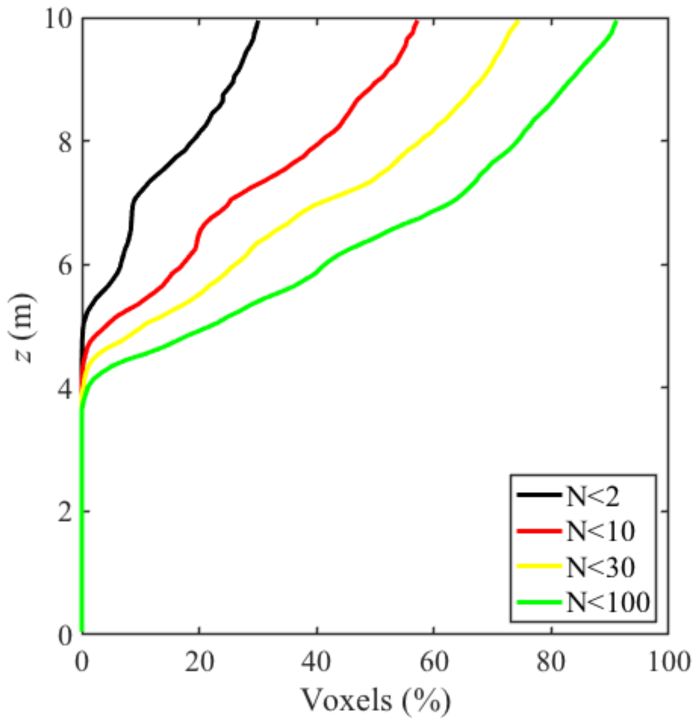

Figure 4. Vertical profiles of percentages of voxels with number of beams smaller than 2, 10, 30 and 100, in the numerical experiment described in Appendix C (5 different view points located at 1 m above the ground).

Preprints (www.preprints.org) | NOT PEER-REVIEWED | Posted: 24 May 2019 doi:10.20944/preprints201905.0287.v1

Peer-reviewed version available at Remote Sensing 2019, 11, ; doi:10.3390/rs11131580

5. Conclusion

The study confirms the potential of the Maximum Likelihood Estimation method for LAD from LiDAR data, as already demonstrated in Pimont et al. (2018), or Zhao et al. (2015) in a slightly different context. The method makes the economy of transmittance computation and inversion as in Beer's law based methods and is more efficient. Here, the estimators for *LAD* in volumes of interest (which can be either voxels or crown volumes, provided that vegetation is randomly distributed inside) are developed in the context where subvolumes can be occupied by wood, with correction factors for vegetation element size, subgrid clumping, LiDAR effective footprint, projection angle and with multiple viewpoints. The new framework can be applied to any multiview dataset in a straightforward manner, such as multiview TLS or UAV LiDAR scanning, provided that a traversal algorithm is available to compute hits and free path distributions, and that the different correction factors (vegetation element size, leaf orientation, leaf hit fraction, calibration factors, and wood volume fraction) are available. A numerical experiment was used to demonstrate the performance of the new estimator, which was favorably compared to other existing methods for the combination of multiple viewpoints. It should lead to less biased and more efficient estimates, provided that at least a few beams explore a voxel.

References

Bailey, B.N., Mahaffee, W.F., 2017a. Rapid, high-resolution measurement of leaf area and leaf orientation using terrestrial LiDAR scanning data. Measurement Science and Technology 28, 064006.

Bailey, B.N., Mahaffee, W.F., 2017b. Rapid measurement of the three-dimensional distribution of leaf orientation and the leaf angle probability density function using terrestrial LiDAR scanning. Remote Sensing of Environment 194, 63–76.

 doi:10.20944/preprints201905.0287.v1

Peer-reviewed version available at *Remote Sensing* **2019**, *11*, ; doi:10.3390/rs11131580

Béland, M., Widlowski, J.L., Fournier, R.A., Cote, J.F., Verstraete, M.M., 2011. Estimating leaf area distribution in savanna trees from terrestrial LiDAR measurements. Agric. For. Meteorol. 151, 1252–1266.

Béland, M., Baldocchi, D.D., Widlowski, J.-L., Fournier, R.A., Verstraete, M.M., 2014a. On seeing the wood from the leaves and the role of voxel size in determining leaf area distribution of forests with terrestrial LiDAR. Agricultural and Forest Meteorology 184, 82–97.

Béland, M., Widlowski, J.-L., Fournier, R.A., 2014b. A model for deriving voxel-level tree leaf area density estimates from ground-based LiDAR. Environmental Modelling & Software 51, 184–189.

Côté, J.F., Fournier, R.A., Egli, R., 2011. An architectural model of trees to estimate forest structural attributes using terrestrial LiDAR. Environ. Model. Softw. 26, 761–777.

Grau, E., Durrieu, S., Fournier, R., Gastellu-etchegorry, J., Yin, T., 2017. Estimation of 3D vegetation density with Terrestrial Laser Scanning data using voxels . A sensitivity analysis of influencing parameters. Remote Sens. Environ. 191, 373–388.

Hu, R., Yan, G., Mu, X., Luo, J., 2014. Indirect measurement of leaf area index on the basis of path length distribution. Remote Sens. Environ. 155, 239–247.

Hu, R., Bournez, E., Cheng, S., Jiang, H., Nerry, F., Landes, T., Saudreau, M., Kastendeuch, P., Najjar, G., Colin, J., Yan, G., 2018. Estimating the leaf area of an individual tree in urban areas using terrestrial laser scanner and path length distribution model. ISPRS J. Photogramm. Remote Sens. 144, 357–368.

Kay, S.M., 1993. *Fundamentals of Statistical Signal Processing: Estimation Theory*, Prentice Hall, 595 p.

Keane, R.E., Reinhardt, E., Gray, K., Reardon, J., Scott, J.H. 2005. Estimating forest canopy bulk density using indirect methods. Can. J. For. Res. 35, 724–739.

Peer-reviewed version available at Remote Sensing 2019, 11, ; doi:10.3390/rs11131580

Li, Y., Guo, Q., Tao, S., Zheng, G., Zhao, K., Xue, B., Su, Y., 2016. Derivation, Validation, and Sensitivity Analysis of Terrestrial Laser Scanning-Based Leaf Area Index. Can. J. Remote Sens. 42, 719–729.

Norman, J.M., Campbell, G.S., 1989. Canopy structure. In: Pearcy, R.W., Ehleringer, J.,Mooney, H.A., Rundel, P.W. (Eds.), Plant Physiological Ecology – Field Methodsand Instrumentation. Chapman and Hall, London, pp. 301–325

Pimont, F., Dupuy, J.L., Caraglio, Y., Morvan, D., 2009. Effect of vegetation heterogeneity on radiative transfer in forest fires. Int. J. Wildl. Fire 18, 536–553.

Pimont, F., Dupuy, J.-L., Rigolot, E., Prat, V., Piboule, A., 2015. Estimating Leaf Bulk Density Distribution in a Tree Canopy Using Terrestrial LiDAR and a Straightforward Calibration Procedure. Remote Sensing 7, 7995–8018.

Pimont, F., Allard, D., Soma, M., Dupuy, J.-L., 2018. Estimators and confidence intervals for plant area density at voxel scale with T-LiDAR. Remote Sens. Environ. 215, 343–370.

Raumonen, P., Kaasalainen, M., Åkerblom, M., Kaasalainen, S., Kaartinen, H., Vastaranta, M., Holopainen, M., Disney, M., Lewis, P., 2013. Fast Automatic Precision Tree Models from Terrestrial Laser Scanner Data. Remote Sensing 5, 491–520.

Soma, M., Pimont, F., Durrieu, S., Dupuy, J.-L., 2018. Enhanced Measurements of Leaf Area Density with T-LiDAR: Evaluating and Calibrating the Effects of Vegetation Heterogeneity and Scanner Properties. Remote Sens. 10, 1580.

Soma, M., Pimont, F., Dupuy, J.-L., 2019. Sensitivity of vegetation structure and sampling limitations on voxel-based estimations of LAD with Terrestrial LiDAR at plot scale: a numerical study. Preprint.

Takoudjou, S.M., Ploton, P., Sonké, B., Hackenberg, J., Griffon, S., Coligny, F. De, Guy, N., Libalah, M., Ii, G., Gilles, M., Moguédec, L., Pélissier, R., Barbier, N., 2018. Using terrestrial laser scanning data to estimate large tropical trees biomass and calibrate allometric models : A comparison with traditional destructive approach. Methods Ecol. Evol. 9, 905–916.

Wang, D., Brunner, J., Ma, Z., Lu, H., Hollaus, M., Pang, Y., 2018. Separating Tree Photosynthetic and Non-Photosynthetic Components from Point Cloud Data Using Dynamic Segment Merging Forest 9, 242.

Xi, Z., Hopkinson, C., Chasmer, L., 2018. Filtering Stems and Branches from Terrestrial Laser Scanning Point Clouds Using Deep 3-D Fully Convolutional Networks. Remote Sensing 10, 1215.

Yan, G., Hu, R., Luo, J., Weiss, M., Jiang, H., Mu, X., Xie, D., Zhang, W., 2019. Review of indirect optical measurements of leaf area index: Recent advances, challenges, and perspectives. Agricultural and Forest Meteorology 265, 390–411.

Zhao, K., García, M., Liu, S., Guo, Q., Chen, G., Zhang, X., Zhou, Y., Meng, X., 2015. Terrestrial lidar remote sensing of forests: Maximum likelihood estimates of canopy profile, leaf area index, and leaf angle distribution. Agric. For. Meteorol. 209-201, 100-113.

 doi:10.20944/preprints201905.0287.v1

Peer-reviewed version available at Remote Sensing **2019**, 11, ; doi:10.3390/rs11131580

Appendix A. Estimation of λ_1 for simple vegetation element shapes

According to Pimont et al. (2018), the attenuation coefficient of a single vegetation element in a cubic voxel of size δ is:

$$\lambda_1 \approx \frac{S_1}{\delta^3} \tag{A1}$$

Where S_1 is the cross-sectional area of a single vegetation element.

For a needle of radius r and length l, this leads to:

$$\lambda_1 \approx \frac{2\pi r l}{4\delta^3} \tag{A2}$$

For a (small) needle of diameter $2r$ = 0.5 mm and length l = 5 cm, we have:

$$\lambda_1 \approx 2\ 10^{-5}\delta^{-3} \tag{A3}$$

For a flat leaf of radius r, this leads to:

$$\lambda_1 \approx \frac{2\pi r^2}{4\delta^3} \tag{A4}$$

For a (large) leaf of diameter $2r$ = 10 cm, we have:

$$\lambda_1 \approx 5\ 10^{-3}\delta^{-3} \tag{A5}$$

Appendix B. Optimized multiview estimator in a voxel of interest

The following derivation generalized the approach suggested in section 3.4 and Appendix C in Pimont et al. (2018). More details on the rationale of the method are provided there.

Here, we assume that we have M scans. We want to compute the ML estimator of LAD, from $\{N_j\}_{j=1,M}$ beams of different scans. For each scan j, the attenuation coefficient λ_j in volume of interest $V - V_w$ corresponds to a projected area of leaf elements equal to $\lambda_j(V - V_w) = c_j LAD\ V$, with $c_j = \frac{G_j}{H_j}$. Hence, $\lambda_j = \frac{c_j LAD}{\alpha}$. The probability distribution of free path z in the voxel in the context of randomly-distributed elements is:

$$f_j(z;\delta) = \begin{cases} \lambda_j(1-\lambda_1 z)^{\lambda_j/\lambda_1 - 1} & (leaf\ hit) \\ (1-\lambda_1\delta)^{\lambda_j/\lambda_1} & (no\ leaf\ hit) \end{cases} \tag{B1}$$

Using the effective path $z_e = -\frac{log(1-\lambda_1 z)}{\lambda_1}$, (B1) can be rewritten:

$$f_j(z;\delta) = \begin{cases} \lambda_j e^{-(\lambda_j-\lambda_1)z_e} & (\text{leaf}\ hit) \\ e^{-\lambda_j z_e} & (no\ leaf\ hit) \end{cases} \tag{B2}$$

Peer-reviewed version available at Remote Sensing 2019, 11, ; doi:10.3390/rs11131580

Let us denote $\left\{{z_e}_j^i\right\}_{i=1,N_j}$ the N_j "effective" free paths of scan j.

From Eq. 1, the likelihood of Z is:

$$\begin{aligned}
\mathcal{L}\left(LAD;\{z_j^i\}_{i=1,N_j \text{ and } j=1,M}\right) &= \prod_{j=1}^{M}\prod_{i=1}^{N_j} f_j\left(z_j^i;\delta_j^i\right) \\
&= \prod_{j=1}^{M}\prod_{leaf\ hits}\lambda_j e^{-(\lambda_j-\lambda_1){z_e}_j^i}\prod_{no\ leaf\ hit} e^{-\lambda_j {z_e}_j^i} \\
&= \prod_{j=1}^{M}\left(\lambda_j^{Ni_j^l}\prod_{i=1}^{N_j} e^{-\lambda_j {z_e}_j^i}\prod_{leaf\ hits} e^{\lambda_1 {z_e}_j^i}\right) \\
&= \prod_{j=1}^{M}\left(\left(\frac{LAD\,c_j}{\alpha}\right)^{Ni_j^l}\prod_{i=1}^{N_j} e^{-\frac{LAD}{\alpha}c_j {z_e}_j^i}\prod_{leaf\ hits} e^{\lambda_1 {z_e}_j^i}\right) \\
&= \left(\frac{LAD}{\alpha}\right)^{Ni^l}\prod_{j=1}^{M}\left({c_j}^{Ni_j}\left(\prod_{i=1}^{N_j} e^{-c_j {z_e}_j^i}\right)^{\frac{LAD}{\alpha}}\prod_{leaf\ hits} e^{\lambda_1 {z_e}_j^i}\right)
\end{aligned} \tag{B3}$$

Where Ni_j^l is the number of leaf hit for scan j and $Ni^l = \sum_j Ni_j^l$ is the total number of hits.

The ML estimator is the value LAD that cancels the first derivative of $\mathcal{L}$ (Kay, 1993, chapter 7). The logarithm of the likelihood is:

$$\begin{aligned}
&log\mathcal{L}\left(LAD;\{z_j^i\}_{i=1,N_j \text{ and } j=1,M}\right) \\
&= Ni^l \log\left(\frac{LAD}{\alpha}\right) + \sum_{j=1}^{M} Ni_j^l \log\left(c_j\right) - \frac{LAD}{\alpha}\sum_{j=1}^{M}\sum_{j=1}^{N_j} c_j {z_e}_j^i + \sum_{leaf\ hits}\lambda_1 {z_e}_j^i
\end{aligned} \tag{B4}$$

Derivating with respect to LAD and equating to zero provides:

$$\frac{dlog\mathcal{L}}{dLAD} = \frac{1}{\alpha}\frac{Ni^l}{\frac{LAD}{\alpha}} - \frac{1}{\alpha}\sum_{j=1}^{M}\sum_{j=1}^{N_j} c_j {z_e}_j^i = 0 \tag{B5}$$

Hence,

$$\mathrm{MLE}_{\mathrm{LAD}} = \alpha\frac{Ni^l}{\sum cz_e} \tag{B6}$$

with $Ni^l = \sum_j Ni_j^l$ the total number of leaf hits et $\sum cz_e = \sum_{j=1}^{M}\sum_{j=1}^{N_j} c_j {z_e}_j^i$ the sum of product $c_j {z_e}_j^i$ for all beams.

Preprints (www.preprints.org) | NOT PEER-REVIEWED | Posted: 24 May 2019 doi:10.20944/preprints201905.0287.v1

Peer-reviewed version available at Remote Sensing 2019, 11, ; doi:10.3390/rs11131580

Hence, the ML estimator (also called modified contact frequency) $\frac{1}{c}\tilde{\lambda} = \frac{I}{cz_e}$ can be generalized to multiple viewpoints.

As explained in Pimont et al. (2018), the MLE exhibits a positive bias when the optical path explored within the voxel is limited. Following supplementary C in Pimont et al. (2018), we can adapt the bias correction to the multiview formulation.

Since $\mathrm{MLE_{LAD}} = \alpha \mathrm{f}(Ni^l, \sum cz_e)$ with $\mathrm{f(x,y)} = \frac{\mathrm{x}}{\mathrm{y}}$, the unbiased estimator $\mathrm{LAD^m}$ can be approximated as:

$$\frac{\widehat{\mathrm{LAD}^{\mathrm{M}}}}{\alpha} = \frac{Ni^l}{\sum cz_e} - \frac{1}{2}\sigma^2_{Ni^l}\frac{\partial^2 f}{\partial x^2}\left(Ni^l, \sum cz_e\right) - \frac{1}{2}\sigma^2_{\sum cz_e}\frac{\partial^2 f}{\partial y^2}\left(Ni^l, \sum cz_e\right) - \sigma_{Ni^l,\sum cz_e}\frac{\partial^2 f}{\partial x \partial y}\left(Ni^l, \sum cz_e\right) \quad \text{(B7)}$$

The different terms can be estimated as follows:

$$-\frac{1}{2}\sigma^2_{Ni^l}\frac{\partial^2 \mathrm{f}}{\partial \mathrm{x}^2}\left(Ni^l, \sum cz_e\right) = -\frac{1}{2}\sigma^2_{Ni^l}\times 0 = 0 \quad \text{(B8)}$$

$$-\frac{1}{2}\sigma^2_{\sum cz_e}\frac{\partial^2 f}{\partial y^2}\left(Ni^l, \sum cz_e\right) = -\sigma^2_{\sum cz}\frac{Ni^l}{(\sum cz_e)^3} \quad \text{(B9)}$$

$$-\sigma_{Ni^l,\sum cz_e}\frac{\partial^2 \mathrm{f}}{\partial \mathrm{x}\, \partial \mathrm{y}}\left(Ni^l, \sum cz_e\right) = \sigma_{\mathrm{Ni},\sum cz_e}\frac{1}{(\sum cz_e)^2} \quad \text{(B10)}$$

We now estimate $\sigma^2_{\sum cz_e} = E[(\sum cz_e)^2] - E[\sum cz_e]^2$ and $\sigma_{Ni^l,\sum cz_e} = E[Ni^l \sum cz_e] - E[Ni^l]E[\sum cz_e]$

Because of beam independency and since $E[\bar{z}^2] = \frac{2}{\lambda}E[\mathbf{1}_{leafhit} z_e]$ (Pimont et al. 2018, Eq. C13) and $\frac{LAD}{\alpha} \approx \frac{Ni^l}{\sum cz_e}$ (Eq. B6):

$$\begin{aligned} E\left[\left(\sum cz_e\right)^2\right] &= \sum_j c_j{}^2 E\left[\sum z_{e_j}{}^2\right] = \sum_j c_j{}^2 N_j E\left[\overline{z_{e_j}}^2\right] \\ &= \sum_j \frac{1}{\lambda_j/1/c_j} 2N_j\, E\left[\mathbf{1}_{leaf\ hit} c_j z_{e_j}\right] \approx \sum_j \frac{\alpha}{\mathrm{LAD}} 2 \sum_{leaf\ hit} c_j z_{e_j} \\ &= \frac{2\alpha}{\mathrm{LAD}} \sum_{leaf\ hit} cz_e \end{aligned} \quad \text{(B11)}$$

Similarly,

$$E\left[Ni^l \sum cz_e\right] = \sum_j E\left[\sum \mathbf{1}_{leaf\ hit} c_j z_{e_j}\right] = \sum_{leaf\ hit} cz_e \quad \text{(B12)}$$

Hence, plugin in Eq. B7:

Preprints (www.preprints.org) | NOT PEER-REVIEWED | Posted: 24 May 2019 doi:10.20944/preprints201905.0287.v1

Peer-reviewed version available at Remote Sensing 2019, 11, ; doi:10.3390/rs11131580

$$\frac{\widehat{\mathrm{LAD}}^{\mathrm{M}}}{\alpha} = \frac{Ni^l}{\sum cz_e} - \left(\frac{2\alpha}{\mathrm{LAD}}\sum_{leaf\ hit} cz_e - \left(\sum cz_e\right)^2\right)\frac{Ni^l}{(\sum cz_e)^3} - \left(\sum_{leaf\ hit} cz_e - Ni^l \sum cz_e\right)\frac{1}{(\sum cz_e)^2} \tag{B13}$$

Hence, since Eq. (B6):

$$\widehat{\mathrm{LAD}}^{\mathrm{M}} = \frac{\alpha}{\sum cz_e}\left(Ni^l - \frac{\sum_l cz_e}{\sum cz_e}\right) \tag{B14}$$

Appendix C. A numerical experiment to compare different Multiview formulations

Method

We conducted a numerical experiment, rather than using actual data, because attributing error source in actual data is often difficult in this research field (Grau et al. 2017; Yan et al. 2019). The goals of this experiment were to i) provide a theoretical validation of the *"M"* –multiview- estimator of *LAD* presented above (Eq. 13), ii) compare its performance with the two usual formulations to combine single-view estimates ("*Nmax*" and "*N-weighted*" $\widehat{LAD}^{Nmax}$ and $\widehat{LAD}^{NW}$, Eq. 4 and 5). We first generated a "reference" *LAD* tridimensional field LAD_{ref} in a mesh grid, with voxels of size equal to 0.1 m, corresponding to a cubic vegetation scene with a 10-m lateral extension and a 10-m height. LAD_{ref} corresponded to a clumped spatial distribution simulated from *RandomFields* R package, which was parameterized to correspond to realistic features of natural vegetation. The mean clump size, which was representative of the tree crown diameter, was 4 m, whereas typical *LAD* vertical profiles, as well as a projection function were implemented. In order to get a more realistic reference field, the random field LAD_{ref} was modified as follows. We multiplied it by a realistic vertical profile, to get limited vegetation under 3 m, and a peak in *LAD* around 7 m height (**Fig. C1a**). Also, the first decile of LAD_{ref} values was set equal to 0 in order to generate actual gaps between crowns. Finally, random variations were also introduced to simulate the occurrence of small gaps (~1 m), representative of branch-scale heterogeneity inside tree crowns. These setting led to a clumped

Preprints (www.preprints.org) | NOT PEER-REVIEWED | Posted: 24 May 2019 doi:10.20944/preprints201905.0287.v1

Peer-reviewed version available at *Remote Sensing* **2019**, *11*, ; doi:10.3390/rs11131580

vegetation scene with a 70% cover fraction and a vertical structuration (**Fig. C1a**). The LAI of the virtual scene was about 3.8, which corresponds to a mean LAD_{ref} of 0.38 m-1 (the scene vertical extent was 10 m). Maximal LAD_{ref} values reached 3.8 m^{-1}.

A leaf projection function was implemented to complete vegetation properties:

$$G(\theta, z) = \frac{1}{2} + 0.4\frac{z}{h}\cos(2\theta) \tag{C1}$$

where θ was the angle between the beams and the vertical, which ranged between 0 and π. According to this setting, leaves were planophile near the canopy top ($z \approx h$), with G=0.9 for vertical beams ($\theta \approx 0$ or $\theta \approx \pi$) and 0.1 for horizontal beams ($\theta \approx \frac{\pi}{2}$), and random near the ground ($z \approx 0$), with G=0.5.

At last, the leaf fraction was parameterized to account for wood and leaf association along the vertical axis following:

$$F(z) = \left(0.1 + 0.8\frac{z}{h}\right)^2 \tag{C2}$$

The leaf fraction was hence equal to 0.9 at canopy top ($z \approx h$) and 0.1 near the ground ($z \approx 0$).

The vertical profile of LAD_{ref}, as well as a two-dimensional horizontal distribution of this vegetation field, are shown in **Fig. C1a&b**. They correspond to a LAI of 3.8 and a cover fraction of 70 %.

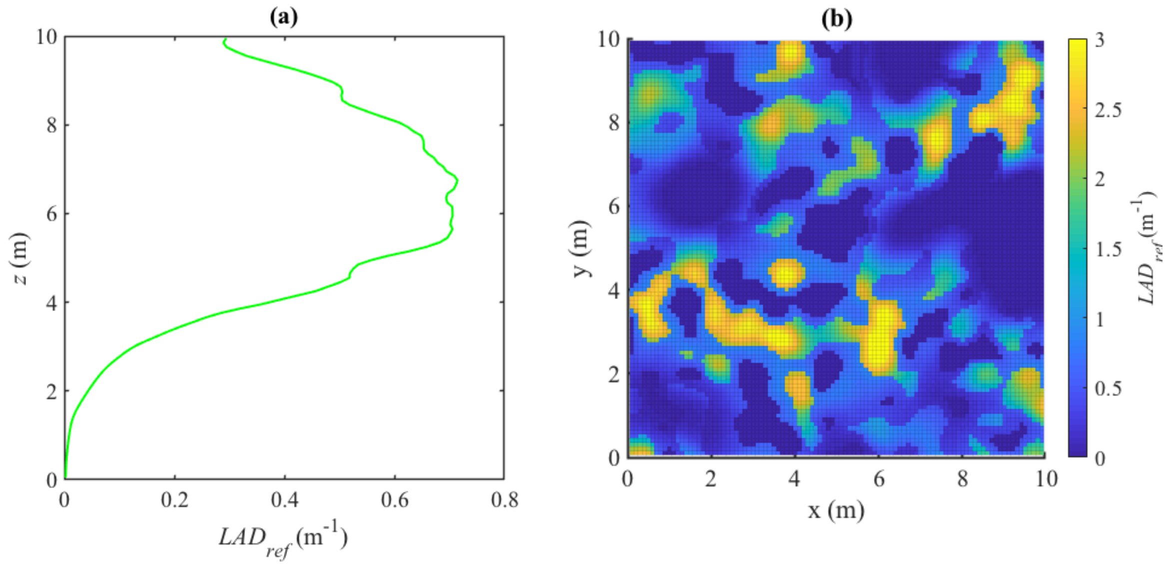

Figure C1. Reference vegetation: (a) vertical profile of LAD_{ref}; (b) horizontal distribution of LAD_{ref} at z=6 m.

We then simulated virtual TLS scans processed at five different locations, with a 0.036° angular resolution. Simulations were based on turbid media assumption (assuming that $\lambda_1 \approx 0$, for simplicity), which states that the probability of a beam to be intercepted increases exponentially with the optical depth (product of attenuation coefficient and distance travelled). For simplicity, the volume fraction of wood elements was neglected ($\alpha = 1$). The locations in which individual laser beams were intercepted were thus generated from random numbers, as in Pimont et al. (2018), but the approach was generalized to a heterogeneous vegetation scene, as in (Pimont et al. 2009).

The reference attenuation coefficient $\lambda_{ref,j}$ related to LAD_{ref} for a given scan j depends on leaf projection, leaf fraction, vegetation heterogeneity and scanner properties (Inverting Eq. 1).

Let (x_j, y_j, z_j) be the coordinates of the scanner corresponding to scan j and (x, y, z) the coordinates of the center of a voxel in the vegetation scene. The effective attenuation coefficient for both leaf and wood for scan j was:

$$\lambda_{ref,j}(x,y,z) = LAD_{ref}(x,y,z)\frac{G_j(x,y,z)}{F(z)H_j(x,y,z)} \tag{C3}$$

A beam emitted from the scanner j in the direction of (x, y, z) had the following projection function G (since $\cos(2\theta) = \cos(\theta)^2 - \sin(\theta)^2$):

$$G_j(x,y,z) = \frac{1}{2} + 0.4\frac{z}{h}\frac{(z-z_j)^2 - (x-x_j)^2 - (y-y_j)^2}{(x-x_j)^2 + (y-y_j)^2 + (z-z_j)^2} \tag{C4}$$

We assumed that the distance effect (caused by an increase in effective footprint of the scanner, as identified in Soma et al. 2018) has the following effect on the attenuation coefficient:

$$H_j(x,y,z) = 1 - 0.05\sqrt{(x-x_j)^2 + (y-y_j)^2 + (z-z_j)^2} \tag{C5}$$

which expressed that leaf area was overestimated by a factor 2 at a distance of 10 m to the scanner (H_j=0.5), which is in agreement with observations of Soma et al. (2018).

We simulated five virtual point clouds corresponding to scanner located at 1 m from the ground and at each corner of the plot and one scan at the center: $(x_1, y_1, z_1) = (7.5,7.5,1)$; $(x_2, y_2, z_2) = (7.5,2.5,1)$; $(x_3, y_3, z_3) = (2.5,2.5,1)$; $(x_4, y_4, z_4) = (2.5,7.5,1)$; $(x_5, y_5, z_5) = (5,5,1)$. Their shooting patterns corresponded to a 0.036° angular resolution over the horizontal (ranging from 0 to 180°) and the vertical (ranging from 0 to 360°), so that each scan contains around 50 million beams, which is typical of the resolution used in the field (e.g. Pimont et al. 2015). For each beam, we simulated its eventual hit location with a ray-tracing algorithm: First, the optical path (i.e. initial potential to pass through vegetation) of each beam was randomly simulated according to the Beer-Lambert law (assuming infinitely small elements, i.e. $\lambda_1 \approx 0$):

$$l = -\log(p) \tag{C6}$$

Peer-reviewed version available at *Remote Sensing* **2019**, *11*, ; doi:10.3390/rs11131580

with p a random number within]0;1], which corresponds to the initial chance to be intercepted by vegetation. We then computed the trajectory of this beam within the computational grid, from its initial position at scanner location, by computing the "amount" of optical path required to cross the next voxel. This amount was calculated by multiplying the reference attenuation coefficient of this voxel (computed from Eq. C3) by the length of the segment corresponding to the intersection of the beam and the voxel. When the residual optical path of the beam was shorter than this amount, a hit occurred within this voxel at a location corresponding to this residual optical path. On the contrary, when the remaining optical path was greater than this amount, it meant that the beam travelled farther than the voxel. The process was recursively applied to the next voxel, the "new" residual optical path corresponding to the remaining of the previous one. The process ended in case of hit, or when a beam reached the bounding box of the computational grid. In this later case, the beam was never intercepted in the computational grid, thus corresponding to a beam with no hit. This process was similar to the one used by (Pimont et al. 2009) to simulate photons trajectories to compute the radiative transfer from a flame through a voxelized heterogeneous vegetation scene with a MonteCarlo approach. Hence, five virtual point clouds were simulated in accordance with $\lambda_{eff,j}$, which accounted for both vegetation and instrument properties.

Finally, we applied a traversal algorithm to each point cloud j to retrieve leaf hits and free path distributions in voxel (size equals to 0.1 m), in order to compute the different statistics required for the different multiview estimators of the LAD. In particular, the number of hits Ni, the number of sampling beams N and the free path lengths of individual beams were computed in each voxel.

We computed the three multiview estimators ($\widetilde{LAD}^{Nmax}$, $\widetilde{LAD}^{NW}$ and $\widetilde{LAD}^{M}$). A two-dimensional horizontal distribution of $\widetilde{LAD}^{M}$ is shown in **Fig. C2** to illustrate these estimates and can be directly compared to **Fig. C1b**. The blank pixels correspond to locations in which

 doi:10.20944/preprints201905.0287.v1

Peer-reviewed version available at *Remote Sensing* **2019**, *11*, ; doi:10.3390/rs11131580

voxels were not sampled by any beam, because of vegetation occlusion. The impact of such occlusion was discussed in details in Soma et al. (2019) and was beyond the scope of the present article.

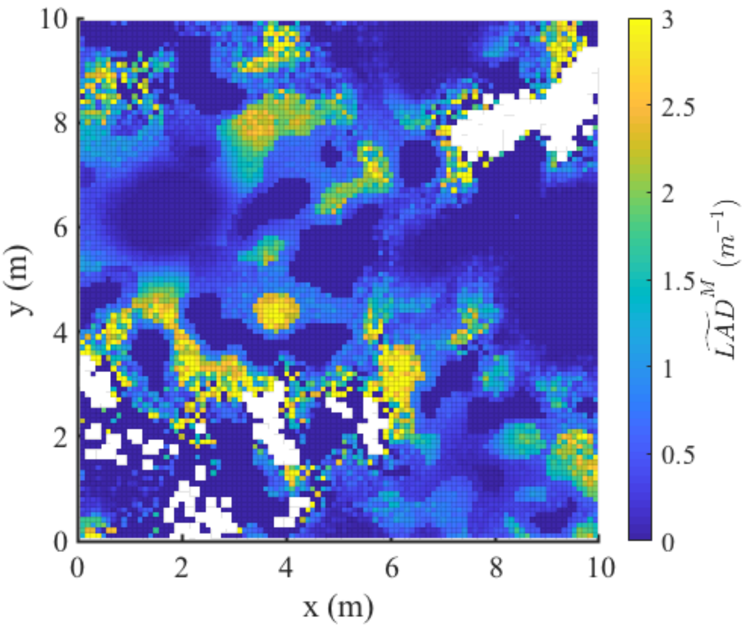

Figure C2. Estimated horizontal distribution of $\widetilde{LAD}^M$ at *z*=6 m. This distribution could directly be compared to LAD_{ref} in **Fig. C1b**. Blank pixels correspond to unexplored voxels, which revealed occluded locations in the canopy.

The performance of the three multiview estimators were compared thanks to reference *LAD* values. We first evaluated their biases, by comparing estimated and reference *LAD* values, grouped per classes of total beam numbers exploring voxels (*N*). Indeed, Pimont et al. (2018) showed that the magnitude of the biases can strongly vary with the number of sampling beams. Then, we computed the Root Mean Square Error (RMSE) of the estimations in individual voxels. As for the bias, RMSE were computed per classes of total beam numbers exploring

Preprints (www.preprints.org) | NOT PEER-REVIEWED | Posted: 24 May 2019 doi:10.20944/preprints201905.0287.v1

Peer-reviewed version available at *Remote Sensing* **2019**, *11*, ; doi:10.3390/rs11131580

voxels (*N*). Both biases and RMSE were expressed in percentage of the mean *LAD* in concerned voxels, in order to ease the interpretation of the results.

Results

The mean biases observed in voxels, computed for three classes of beam number *N*, are shown in **Table C1**. With the new multiview estimator ($\widetilde{LAD}^M$), biases were smaller than 1 % for $N \geq 10$ and were only equal to 2.2% when $N < 10$. The two other estimates exhibited biases of larger magnitudes, especially the "*N-weighted*" estimates (*NW*), which reached -15 % when $N < 10$. Such a result was quite surprising: as a weighted average of unbiased estimators (computed for each scan), one would have expected the *NW* estimator to be unbiased too. There was a simple explanation to this apparent paradox: when *N* was smaller than 10, it often corresponded to cases where the beam number exploring a voxel from one or several viewpoints was smaller than 5 and in particular equal to 1 or 2. In these cases, the single-view estimator was negatively biased (Pimont et al. 2018). For example, this bias was especially obvious when *Nj*=1 (in this case, it is equal to 0 when Ni^l=0, but also when Ni^l =1, since $\frac{\sum_l z_e}{\sum z_e}$=1, see Eq. 5).

Table C1. Mean biases (in % of the mean LAD_{ref}) of the three estimators for three different classes of total beam number *N*.

Range of beam number	$\widetilde{LAD}^{Nmax}$	$\widetilde{LAD}^{NW}$	$\widetilde{LAD}^{M}$
$N \geq 2\ and\ N < 10$	-6.0 %	-15 %	+2.2 %
$N \geq 10\ and\ N < 15$	+0.8 %	-2.8 %	+0.4 %
$N \geq 15$	+0.0 %	-0.4 %	+0.0 %

The RMSE observed in voxels, computed for six classes of beam number *N* are shown in **Table C2**. With the multiview estimator ($\widetilde{LAD}^M$), RMSE were smaller than those of the two other estimates. In particular, differences between $\widetilde{LAD}^{M}$ and $\widetilde{LAD}^{Nmax}$ were observed for all classes of beam numbers and were explained by the fact that the information from secondary viewpoints was ignored with "*Nmax*", leading to larger RMSE. Differences between $\widetilde{LAD}^{M}$ and $\widetilde{LAD}^{NW}$ mostly occurred for N ranging between 10 and 30, but RMSE for $\widetilde{LAD}^{NW}$ could be more than twice as big as for $\widetilde{LAD}^{M}$. More detailed analyses (not shown) show that these strong differences in performances were caused by a very limited number of voxels in which errors of $\widetilde{LAD}^{NW}$ were very high, when compared to those of $\widetilde{LAD}^{M}$. This occurred when one of the $\widetilde{LAD}_j$ estimates with a very low number of beams (*Nj* lower than 5) was very far beyond the reference value (for example, when the mean free path from viewpoint *j* was unluckily very small for the *Nj* beams). In this configuration, very large overestimations could occur for the *"N-weighted"* estimator, despite of the weighting procedure, which was not able to dampen such outliers. As a result, the "*NW*" estimator led to higher RMSE than the "*Nmax*", despite more information was used, which highlights the limits of the *NW* formulation.

Table C2. Root Mean Square Error (in % of the mean *LAD*) of the three multiview estimators for six different classes of total beam numbers.

Range of beam number	$\widetilde{LAD}^{Nmax}$	$\widetilde{LAD}^{NW}$	$\widetilde{LAD}^{M}$
$N \geq 2\ and\ N < 10$	450 %	410 %	416 %
$N \geq 10\ and\ N < 15$	137 %	234 %	114 %
$N \geq 15\ and\ N < 30$	99 %	183 %	83 %
$N \geq 30\ and\ N < 100$	61 %	52 %	51 %
$N \geq 100\ and\ N < 1000$	37 %	31 %	30 %